Journal of Materials Processing Technology 228 (2016) 59–67

Journal of Materials Processing Technology

journal homepage: www.elsevier.com/locate/jmatprotec

Modelling kinetics of phase transformation for the indirect hot stamping process to focus on car body parts with tailored properties

Paul Hippchen[a], Arnulf Lipp[a], Hannes Grass[a], Philipp Craighero[a], Michael Fleischer[a], Marion Merklein[b,*]

[a] BMW Group, 80788 München, Germany
[b] Friedrich-Alexander-Universität Erlangen-Nürnberg, 91058 Erlangen, Germany

ARTICLE INFO

Article history:
Received 22 July 2014
Received in revised form
26 November 2014
Accepted 9 January 2015
Available online 19 January 2015

Keywords:
Indirect hot stamping process
Material modelling
Kinetics of phase transformation

ABSTRACT

To design the indirect hot stamping process, a finite element method (FEM) based prediction of the part geometry and the mechanical properties is required. In case of indirect hot stamping processes, producing car body parts with tailored properties, cooling paths occur causing diffusionless and diffusion controlled phase transformations. The volume expansion caused by the phase transformation of face-centred cubic (fcc) into body-centred cubic (bcc) and the martensitic formation of body-centred tetragonal (bct) leads to transformation induced strains that are important for the calculation of overall stresses in hot stamped car body parts. To calculate the strain and stress state correctly, it is necessary to model the diffusionless and diffusion controlled phase transformation phenomena, taking into account the boundary conditions of indirect hot stamping processes. The existing material models are analysed and extended in order to improve their prediction accuracy in calculating the amount and distribution of ferrite, perlite, bainite and martensite during the whole process of annealing. For industrial use the new approaches are implemented in the FE-code LS-DYNA 971 (Livermore Software Technology Corporation, 2006).

1. Introduction

The use of the finite element method has received a lot of attention over the past several years, especially regarding the design of hot stamping processes (Finkler et al., 2013) and for manufacturing car body parts with tailored properties that are described by Banik et al. (2011). The hot stamping process describes a heat treatment process of the mainly used material 22MnB5. The aim of this process must be the manufacturing of weight optimized car body parts meeting the respective specific requirements of structural complexity and strength for a good crash performance by using the mechanisms of phase transformation in steel by different process techniques described by Mori (2012). Therefore an austenitized blank is simultaneously formed and quenched (direct hot stamping) or a cold formed car body part is austenitized and quenched (indirect hot stamping) in a cooled tool. In dependency on the temperature history, different phase transformations from austenite into ferrite, perlite, bainite and martensite can occur (Karbasian and Tekkaya, 2010). The complexity of the occurring phase transformations in steel can be described by numerical approaches that are discussed by Olle (2010) and Behrens et al. (2012) or that are implemented in commercial material models like *MAT_244 (Livermore Software Technology Corporation, 2014) in the FE-code LS-DYNA 971 developed by Livermore Software Technology Corporation (2006). This material model, developed by Åkerström (2006), is primarily used for the prediction of the amount and distribution of ferrite, perlite, bainite and martensite for calculating the mechanical properties of hot stamped car body parts like those with tailored properties as described by George et al. (2011).

Analyses by Hippchen et al. (2012a,b) regarding the kinetics of the formation of martensite have shown that an alternative approach is necessary, especially to focus on car body parts with tailored properties. This is recommended out of the reason that the presented approach was not designed to calculate the kinetics of phase transformation for the combination of diffusionless and diffusion controlled formed phases. To model diffusionless phase transformations according to the boundary conditions of an indirect hot stamping process a new martensite model was developed which is introduced in this study.

Further analyses to material model *MAT_244 (Livermore Software Technology Corporation, 2014) have shown that the

* Corresponding author. Tel.: +49 91318527140.
E-mail addresses: paul.hippchen@bmw.de (P. Hippchen), arnulf.la.lipp@bmw.de (A. Lipp), hannes.grass@bmw.de (H. Grass), philipp.craighero@bmw.de (P. Craighero), michael.ma.fleischer@bmw.de (M. Fleischer), marion.merklein@fau.de (M. Merklein).

http://dx.doi.org/10.1016/j.jmatprotec.2015.01.003

diffusion controlled phase transformation phenomena cannot be modelled close to the measured data of material tests performed in dilatometric testing by Hippchen et al. (2012a); thus the study describes an approach calculating the mechanical properties and geometry of indirect hot stamped car body parts with tailored properties by coupling the diffusion controlled kinetics of phase transformation with a thermo-mechanically coupled material model. The aim is to consider the composition of the volume fractions, phase transformation induced strain and plasticity, and hardening over the entire process of annealing. This is mandatory for calculating overall strains and stresses for springback simulation immediately after the hardening process and for the simulation of thermal deformations while supercooling to room temperature.

2. Examined material

The examined material 22MnB5 (HC380WD + Z140), a fine grained boron manganese steel with zinc coating, is produced by Voestalpine Stahl GmbH (2014) known under the name of phs-ultraform 1500 Z140. The initial blank thickness is 1.5 mm. The measured chemical composition is shown in Table 1.

The average austenite grain size is $d = 8\,\mu m$. It was analysed in metallographic examinations by etching after Bechet Beaujard (2003). The austenite grain size corresponds to $G_{ASTM} = 11$. It is autonomous from the effective plastic strain which is induced by a cold forming process due to the indirect hot stamping process. The thermal properties of this material such as conductivity, specific heat and the thermo-mechanical properties can be found in Hochholdinger (2012).

3. Experimental setup and corresponding simulation model

The experimental investigations to the kinetics of phase transformation were performed in dilatometric testing in a BÄHR DIL 805A/D (BÄHR-Thermoanalyse GmbH, 2014). Taking into account the boundary conditions of an indirect hot stamping process the time dependent temperature curves of an indirect hot stamping process were analysed (Fig. 1(a)). Additionally, investigations to the microstructure and measurements of retained austenite, using the Joch-Isthmus-Method as described by Zhao et al. (2001), were conducted.

In order to investigate the quality of prediction of material model *MAT_244 (Livermore Software Technology Corporation, 2014), which is implemented in the FE-code LS-DYNA 971, relating to the experimental setup a FE-model is used. It is based on a single element test as shown in Fig. 1(a). The time dependent temperature curves measured in dilatometric testing are modelled by a Dirichlet boundary condition. The FE-model is solved considering thermo-mechanical coupling with a fully integrated four node shell-element (Bathe, 2002) using thermal-shell option (Bergman and Oldenburg, 1997, 2004) and integration points across the shell thickness (Fig. 1(b)).

4. Modelling diffusionless kinetics of phase transformation

The modelling of diffusionless kinetics of phase transformation by means of the finite element method is an important step in calculating transformation induced strains and stresses to focus on springback simulation in indirect hot stamping processes.

Regarding the approach of Koistinen and Marburger (1959), which is state of the art in modelling diffusionless kinetics of phase transformation, the progress of phase transformation cannot be approximated in dependency on the supercooling in a sufficient accuracy (Fig. 2(left)) (Hippchen et al., 2012b). The experimental results are shown for an average cooling rate between 800 °C and 500 °C of 100 K/s that represents a martensitic phase transformation. All other cooling rates analysed in this work are defined between 800 °C and 500 °C.

Consequently a new approach was introduced using the constitutive equation of Lee et al. (2010) for modelling diffusionless kinetics of phase transformation. Since the formation of martensite is a time-independent process, Eq. (1) shows a rate based approach to the temperature T describing the formation of martensite (m) as a sigmoid function (Fig. 2(right)). Here, ζ_m is the volume fraction of martensite, M_s the martensite start temperature and T the current temperature. The parameters α, n, φ_m and ψ_m are material model parameters that influence the incubation time and the rate of formation $d\zeta_m/dT$ in dependency to the austenite grain size (Lee et al., 2010). The austenite grain size corresponds to $G_{ASTM} = 11$ and the martensite start temperature is 410 °C.

$$\frac{d\zeta_m}{dT} = \alpha(M_s - T)^n \zeta_m^{\varphi_m}(1-\zeta_m)^{\psi_m} \tag{1}$$

To use the model proposed by Lee et al. (2010) also for processes and cooling paths with a previous formation of diffusion controlled volume fractions it is mandatory to model the rate of formation of martensite $d\zeta_m/dT$ with a normalized fraction ξ_m called the ghost fraction as shown in Eq. (2). Otherwise the sum of diffusion controlled and diffusionless formed volume fractions will be greater than 100 vol%.

$$\frac{d\xi_m}{dT} = \alpha(M_s - T)^n \xi_m^{\varphi_m}(1-\xi_m)^{\psi_m} \tag{2}$$

Subsequently, the ghost fraction ξ_i, which can be a value between 0 and 1, has to be balanced to the amount of retained austenite ζ_γ at martensite start temperature M_s. This is necessary to get the real amount of martensite ζ_m as defined by Eq. (3).

$$\zeta_m = \xi_m \zeta_\gamma | \zeta_\gamma = 1 - \zeta_f - \zeta_p - \zeta_b|_{T=M_s} \tag{3}$$

Depending on the amount of diffusion controlled formed volume fractions, the rate of formation must be updated taking into account the effect of carbonization of retained austenite. Therefore the rate of Eq. (2) is extended by a linear term in its exponent that describes the saturation of the formation of martensite in dependency on the amount of retained austenite ζ_γ at martensite start temperature M_s Eq. (4).

$$\frac{d\xi_m}{dT} = \alpha(M_s - T)^n \xi_m^{\varphi_m}(1-\xi_m)^{\psi_m(2-\zeta_\gamma)} | \zeta_\gamma = 1 - \zeta_f - \zeta_p - \zeta_b|_{T=M_s} \tag{4}$$

The material model parameters α, n, φ_m and ψ_m were identified for a cooling rate of 100 K/s by using the methods of optimization, for example evolutionary strategies, as described by Hippchen et al. (2013). Subsequently, the linear term was found by numerical modelling using the measurement data of retained austenite at room temperature in dependency on the analysed average cooling rates from 100 K/s to 5 K/s. The slightest amount of retained austenite is 1.1 vol% at an average cooling rate of 100 K/s. The highest amount is 4.0 vol% at an average cooling rate of 10 K/s and 5 K/s.

As exemplarily shown in for an average cooling rate of 30 K/s, the transformation of austenite (Fig. 3(left)) and the rate of transformation of austenite (Fig. 3(right)) can be calculated during the whole process of annealing close to the measured data also for lower cooling rates.

Additionally, the amount of retained austenite at room temperature can be predicted which is an indicator for the end of the phase transformation. This information can be used for efficient process design for the determination of the minimum holding time while hardening for example. Fig. 3(left) also shows that a greater supercooling below the martensite start temperature is necessary for cooling rates with diffusion controlled phase transformations in

Table 1
Measured chemical composition for HC380WD + Z140.

Element	C	Si	Mn	P	Al	Cr	Ni	V	B	Ti
wt%	0.207	0.190	1.240	0.008	0.005	0.216	0.015	0.004	0.003	0.033

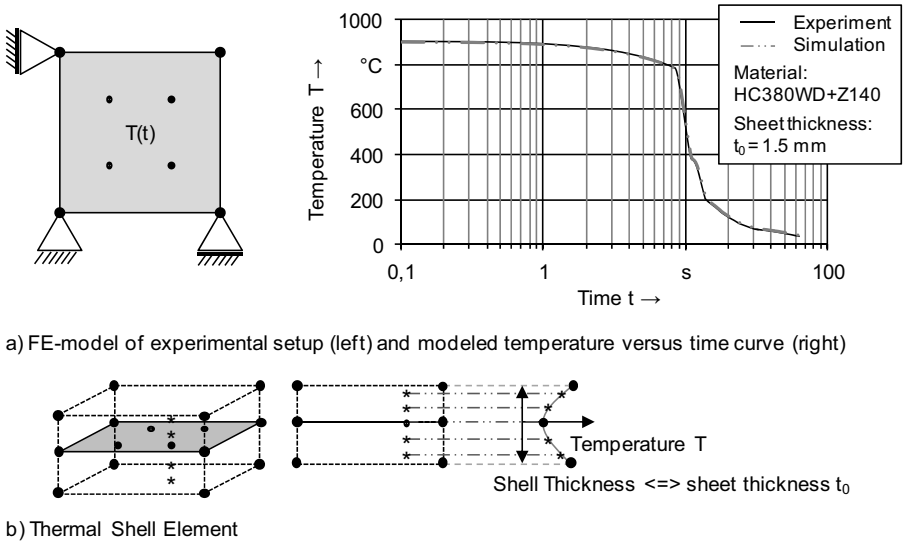

Fig. 1. (a) The FE-model of experimental setup modelling the time dependent temperature curve of an indirect hot stamping process by a Dirichlet boundary condition and (b) use of the thermal-shell-element.

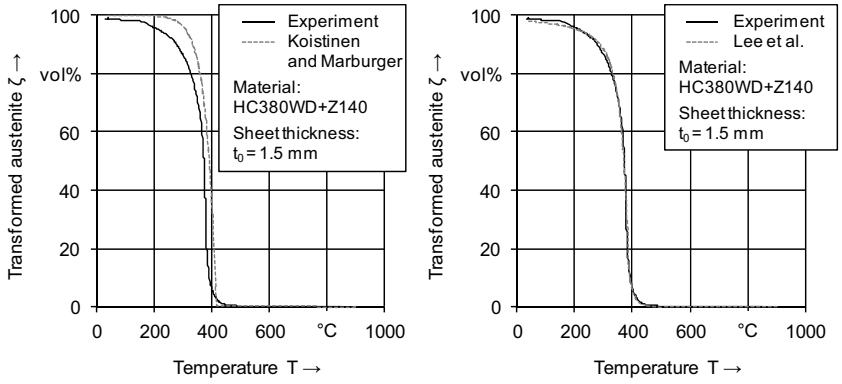

Fig. 2. Martensite formation in dependency on supercooling the martensite start temperature M_s using the approach by Koistinen and Marburger (1959) (left) and Lee et al. (2010) (right).

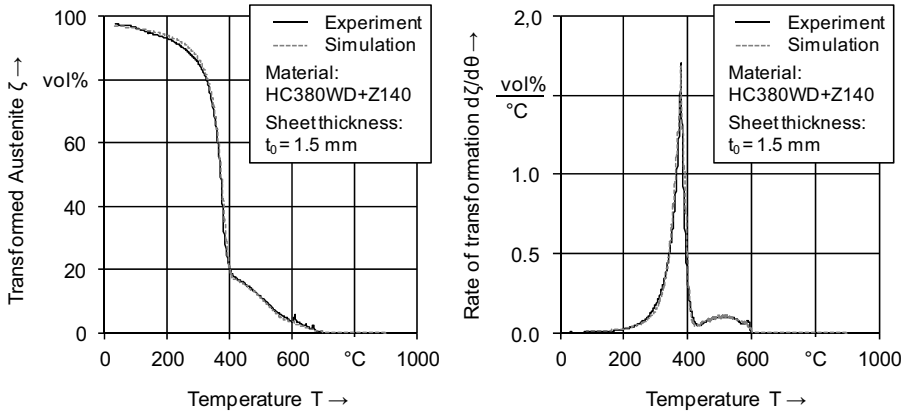

Fig. 3. Transformation of austenite (left) and rate of transformation of austenite (right) for an average cooling rate of 30 K/s.

order to gain for a full transformation of austenite. This is due to the carbonization of retained austenite.

Fig. 3 also indicates that higher cooling rates are necessary for a full martensitic phase transformation as shown in Fig. 2. The experimental results of dilatometer tests have shown that an average cooling rate (measured between 800 °C and 500 °C) greater than 70 K/s is mandatory to form nearly 100 vol% of martensite. It was investigated regarding the boundary conditions of an indirect hot stamping process. Thus the cooling rate of 70 K/s is defined as the upper critical cooling rate for the examined material. This is due to the fact that an industrial hot stamping process is not a process of one continuous cooling condition. Furthermore it is a process with different continuous cooling conditions taking into account for each step (part transfer/tool closing, press hardening and cooldown) of the indirect hot stamping process as shown in Fig. 1(a).

5. Modelling diffusion controlled kinetics of phase transformation

The calculation of diffusion controlled kinetics of phase transformation by means of finite element method is one of the key elements for the prediction of mechanical properties and geometry of hot stamped car body parts with tailored properties. Therefore the hardening effects and the strains, dependent to the diffusion controlled phase transformation phenomena, must be considered correctly. Thus the amount and distribution of ferrite (f), perlite (p), and bainite (b) must be known during the whole process of annealing.

The time dependent decomposition of austenite can be calculated by the approach of Kirkaldy and Venugopalan (1983) as a function of the austenite grain size G_{ASTM}, the chemical composition C_i, the temperature in equilibrium $T_{eq,i}$, and the formed phase itself ξ_i Eq. (5). The parameter Q_i describes the individual activation energy of each phase, R is defined as the universal gas constant and T stands for the current temperature.

$$\frac{d\xi_i}{dt} = 2^{(G_{ASTM}-1)/2}\frac{\exp\left(-Q_i/RT\right)}{C_i}(T_{eq,i}-T)^n\xi_i^{2/5(1-\xi_i)}(1-\xi_i)^{2/5\xi_i} \tag{5}$$

Åkerström (2006) firstly used the phase transformation model to calculate the decomposition of austenite into ferrite (f), perlite (p), and bainite (b) for hot stamping processes. Therefore ξ_i was introduced as a ghost fraction, taking into account more than two different phases. The true amount of each phase ζ_i will be calculated, taking into account the amount of ferrite in equilibrium in dependency on the supercooling Eq. (6).

$$\zeta_f = \xi_f\zeta_{eq,f} \quad \text{and} \quad \zeta_i = \xi_i(1-\zeta_{eq,f})|i = p, b \tag{6}$$

As implemented in the FE-code LS-DYNA the amount of ferrite in equilibrium is calculated in material model *MAT_244 (Livermore Software Technology Corporation, 2014) by using the material dependent phase diagram (Fig. 4(left)). As a result the amount of ferrite does not change below A_{e1}-temperature. Independent of the supercooling below the A_{e1}-temperature the same amount of ferrite will be predicted reckoning a diffusion controlled phase transformation (Fig. 5(left)).

The changed mechanisms in the formation of ferrite (f) and perlite (p) due to the supercooling of austenite are not taken into account calculating the decomposition of austenite (γ). Therefore the material dependent phase diagram is modified by the extrapolation of Hultgren (1938) according to the isothermal phase diagram (Fig. 4(right)).

The use of the extrapolation of Hultgren (1938) can be constituted by the mechanisms of the formation of ferrite (f) and perlite (p). The formation of proeutectoid ferrite leads to a diffusion process of carbon into the austenite region which is casual for a rise of the amount of carbon in austenite. When the solubility of carbon in austenite is reached, the formation of perlite starts.

Due to the supercooling of austenite, which occurs in an indirect hot stamping process, the effect of a change in the lattice constant of austenite must be considered to the solubility of carbon in austenite. Therefore the A_z- and A_3-lines are extrapolated as suggested by Hultgren (1938). Likely to the conditions in equilibrium, proeutectoid ferrite is formed until the solubility of carbon in austenite is reached, but now it is modelled in dependency on the supercooling (Fig. 5(right)).

The phase diagram considering the extrapolation of Hultgren (1938) for supercooling the A_{e1}-temperature in equlibrium can be calculated by Eqs. (7)–(9). Here T_c stands for the temperature point in the phase diagram where no proeutectoid ferrite is formed, C_{fZ} describes the carbon solubility line of ferrite in zementite and $C_{\gamma Z}$ describes the carbon solubility line of austenite in zementite.

$$T_c = T_E - (T_E - A_{e1})\left(\frac{C_E - C_C}{C_E - C_S}\right) \tag{7}$$

$$C_{fz}(T) = C_P - (C_P - C_Q)\left(\frac{A_{e1} - T}{A_{e1} - T_Q}\right) \tag{8}$$

$$C_{\gamma z}(T) = C_S - (C_S - C_C)\left(\frac{A_{e1} - T}{A_{e1} - T_C}\right) \tag{9}$$

By the use of this model the true amount of ferrite (f) and perlite (p) can be calculated by Eq. (6) balanced to the amount of the ghost fractions ξ_i. Besides the modelling of the formation of ferrite in equilibrium, the accuracy in predicting the phase transformation kinetics depends on the rate dependent calculation of the ghost fraction ξ for each phase i.

To model diffusion controlled phase transformations for continuous cooling conditions with a constant cooling rate, the approach of Kirkaldy and Venugopalan (1983) is used in the FE-code LS-DYNA 971 in a modified configuration according to Li et al. (1998). It is state of the art in modelling diffusion controlled phase transformations for hot stamping processes. Since industrial hot stamping processes are not processes with continuous cooling conditions, as seen in Fig. 1(a) it is necessary to control the incubation time and the rate of decomposition in dependency on the cooling conditions according to the industrial set up. Therefore the material model parameters must be identified, taking into account the boundary conditions of the indirect hot stamping process and the individually used material as described by Hippchen et al. (2013). Eq. (5) will be parameterized by the introduction of the grain size parameter ω_i and the specific transformation kinetic parameters φ_i and Ψ_i that can be set individually for each phase in order to calculate the ferrite, perlite, and bainite formation (Eq. (10)).

In experimental set up it could be analysed that the incubation times are dependent on the cooling rate. So, a retardation coefficient C_r is introduced for each phase and the material model is extended to a cooling rate dependency for the parameter φ_i and C_r defined by Eq. (11). Consequently, the cooling rate dependent effects by supercooling austenite can be taken into account on the carbon diffusion.

$$\frac{d\xi_i}{dt} = 2^{\omega_i G_{ASTM}}\frac{\exp\left(-Q_i/RT\right)}{C_i}(T_{eq,i}-T)^n\frac{\xi_i^{\varphi_i(1-\xi_i)}(1-\xi_i)^{\psi_i\xi_i}}{\exp(C_{r,i}\xi_i^2)} \tag{10}$$

with

$$\varphi_i = \varphi_i\left(\frac{dT}{dt}\right) \quad \text{and} \quad C_{r,i} = C_{r,i}\left(\frac{dT}{dt}\right)|i = f, p, b \tag{11}$$

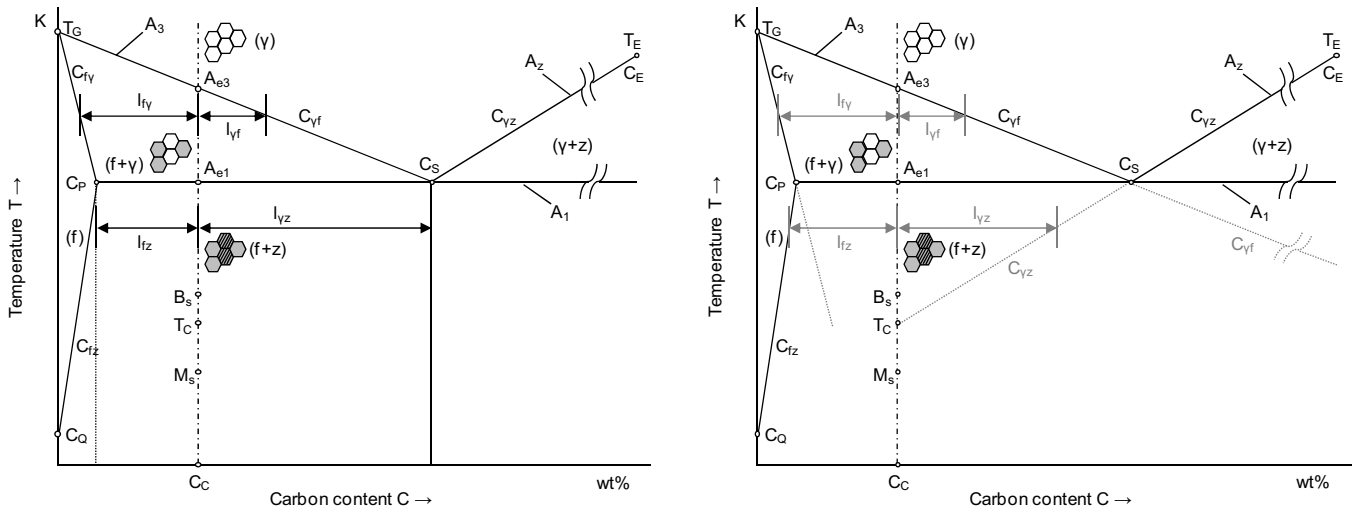

Fig. 4. Material dependent phase diagram (left) and material dependent phase diagram modified by the extrapolation of Hultgren (1938) (right).

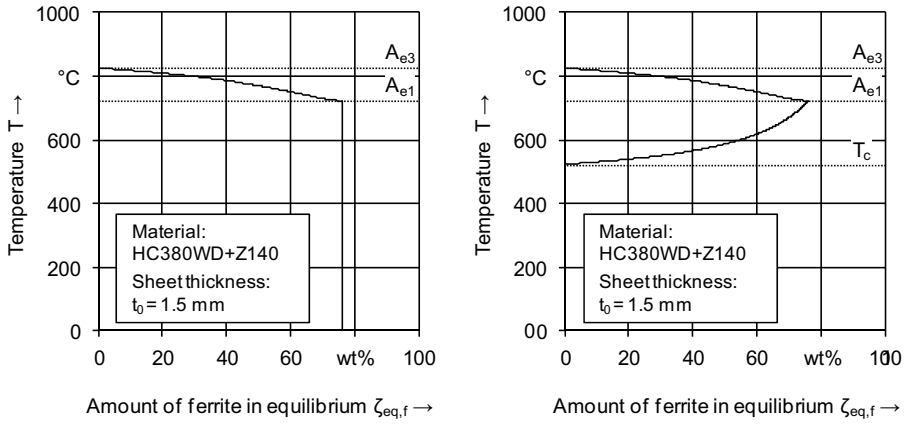

Fig. 5. Development of the amount of ferrite in equilibrium in wt% calculated regarding the material dependent phase diagram (left) and development of the amount of ferrite in equilibrium considering the material dependent phase diagram modified by the extrapolation of Hultgren (1938) (right).

By introducing this extension the continuous cooling transformation can be calculated dynamically in dependency on the predominant cooling rate. It is shown schematically by the development of the time temperature transformation diagram (Fig. 6(left)) and the incubation time (Fig. 6(right)), influenced by the parameter φ_i.

Taking into account the extrapolation of Hultgren (1938) and a cooling rate dependency, the suppressed formation of ferrite at greater cooling rates can be calculated close to the results of dilatometric testing. For the investigated material the cooling rate dependent transformation kinetic parameters for ferrite φ_f are listed in Table 2.

Thus, it is possible to model the kinetics of diffusion controlled phase transformations even for greater (Fig. 7(left)) and lower cooling rates (Fig. 7(right)).

The suppressed and delayed formation of volume fractions can be explained by a suppressed diffusion of carbon due to a fast supercooling of austenite. In a hot stamping process the speed of

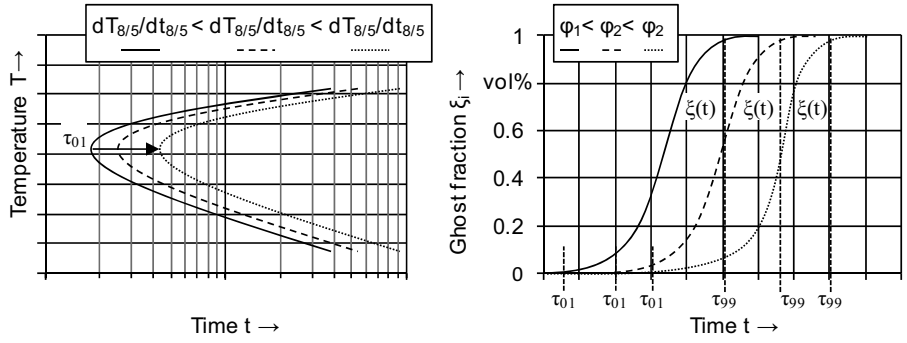

Fig. 6. Development of the time temperature transformation diagram (left) and development of the incubation time (right), influenced by the parameter φ_i, in dependency on the cooling rate.

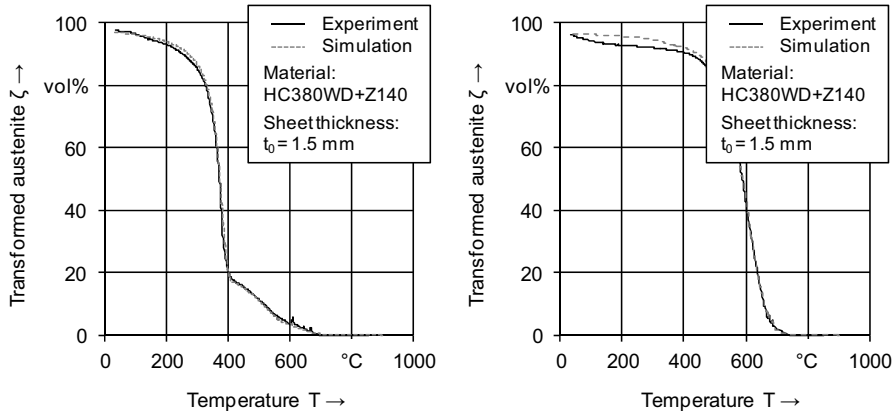

Fig. 7. Kinetics of phase transformation for two different cooling rates (left $dT_{8/5}/dt_{8/5}$ = 30 K/s|right $dT_{8/5}/dt_{8/5}$ = 10 K/s).

supercooling is dependent on the contact conditions during the hardening process; for this reason the overall quality of prediction of the kinetics of phase transformation is dependent on the prediction of the time–temperature evolution which is dependent on the entire FE-model representing the whole process of hot stamping close to the industrial setup.

6. Industrial application

For industrial application the new approaches in modelling diffusionless and diffusion controlled kinetics of phase transformation were implemented in the FE-code LS-DYNA 971 and will be released as material model *MAT_248. This material model can be used for each heat treatment process on steel. For research activities on new materials a default for the transformation kinetic parameters of the diffusion controlled transformation can be chosen in accordance to material model *MAT_244. The transformation kinetic parameters for the diffusionless phase transformation can be chosen as proposed for material model *MAT_248 in Livermore Software Technology Corporation (2014). A method to find the transformation kinetic parameters for each single material is shown in Hippchen et al. (2013).

Additionally, an approach for the calculation of phase dependent strains is implemented by Eq. (12) (Trapp, 2010). It is based on the change of density $d\rho$ due to a phase transformation from fcc into bcc.

$$d\varepsilon_{tr_{mn}} = \frac{-1}{3(\rho + d\rho)} \sum_{1}^{n} d\zeta_i \rho_i \delta_{mn} | i = \gamma, f, p, b, m \tag{12}$$

The density can be calculated using the models of Jablonka et al. (1991) and Miettinen (1997). Alternatively, the density can be set individually for each phase as a data field input by measured data where ρ stands for the density at room temperature and ρ_i stands for the density of each phase.

To validate the material model for industrial use, the numerical results were compared to those of the experimental setup for different types of hot stamped car body parts. The experiments were performed in industrial environment taking into account all boundary conditions of the industrial setup of an indirect hot stamping process. The part geometry shown in this work represents a prototype of a b-pillar, taking into account all features characteristically for the indirect hot stamping process focusing on car body parts with tailored properties.

Table 2
Cooling rate dependent transformation kinetic parameter φ_f to calculate the incubation time of ferrite.

Cooling rate	>10 K/s	≤10 K/s
Parameter	$\varphi_{f,1}$	$\varphi_{f,2}$
Value	0.62	0.42

Fig. 8 displays the results from the metallographic analysis regarding the volume fractions of the indirect hot stamped b-pillar with tailored properties. The microsections 1 and 2 (Fig. 8(b)) are taken from the part area with graded mechanical properties (Fig. 8(a)). Due to an air gap which is defined in the hot stamping tool, the cooling rate could be reduced significantly. The reduction of the cooling rate to 15 K/s (microsection 1) results in a ferritic–perlitic–baintitic microstructure. A marginal faster cooling rate of 18 K/s (microsection 2) results in higher amounts of bainite.

Analogical to the analysis of the polished microsections (Fig. 8), a clear differentiation of ferrite, perlite, and bainite can be conducted with material model *MAT_248 (Fig. 9), due to the modelling of the diffusion controlled kinetics of phase transformation taking the extrapolation of Hultgren (1938) and the rate Eqs. (4) and (10) into consideration.

Contrary to material model *MAT_248, material model *MAT_244 (Livermore Software Technology Corporation, 2014) overpredicts the amount of ferrite significantly as the difference plots show in Fig. 10. The volume fractions of perlite and bainite are underpredicted. This leads to a wrong prediction of mechanical properties.

In this context Fig. 11 shows the predicted Vickers hardness of both material models, by using the Maynier model, in comparison to the measured data. In the analysed sections (Fig. 11(a)) the predicted values of the minimum Vickers hardness in section planes 1 and 3 are about 135 HV10 with material model *MAT_244 (Livermore Software Technology Corporation, 2014) while *MAT_248 predicts values between 170 HV10 and 180 HV10 which are close to the measured data of 175 HV10 (Fig. 11(b)). The build-up of the Vickers hardness at 25 mm of the specimen, that can be seen in section plane 2, is caused by a point of geometric support in the tool that is predicted by both material models in good approximation to the measured data.

Due to the prediction of the volume fractions close to reality the hardening effects of perlite and bainite can be taken into account in the prediction of the part geometry with the material model *MAT_248. To point up the hardening effect, the calculated yield curves of ferrite, perlite, and bainite at a temperature of 300 °C are shown in Fig. 12 in dependency on the effective plastic strain. It can be seen that the yield stress k_f of the perlitic and bainitic phases have a significant higher level in comparison to the ferritic phase. Using a mixture rule

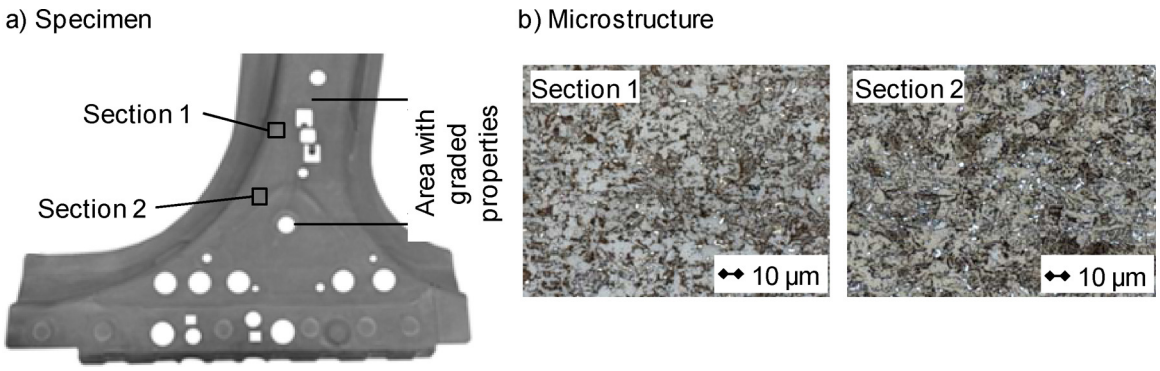

Fig. 8. (a) Specimen and location of microsections and (b) investigated microstructure in sections 1 and 2.

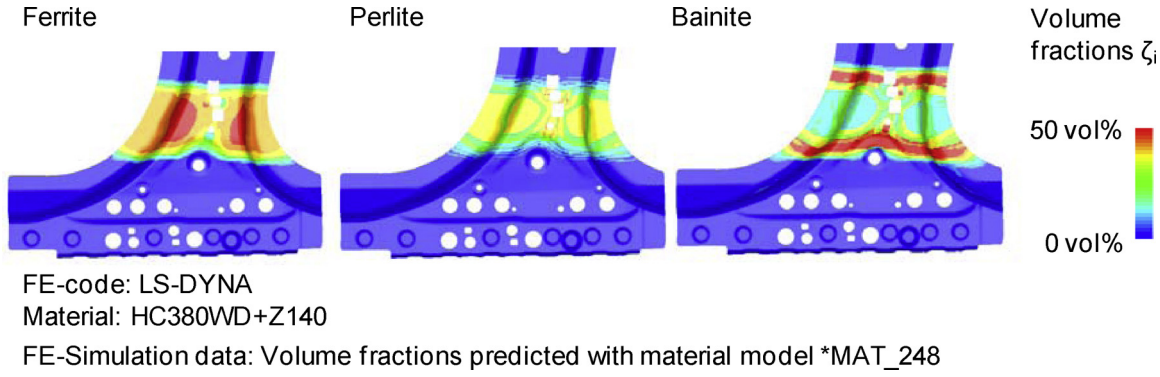

Fig. 9. Predicted volume fractions of ferrite, perlite and bainite due to a diffusion controlled phase transformation with material model *MAT_248.

(Eq. (13)) the resultant yield curve $k_f(\varepsilon_{pl})$ can be calculated as a function of yield stress k_f and the existing volume fractions ξ_i at each temperature. This is necessary, taking the hardening effects over the entire process of annealing into consideration.

$$k_f = \sum_{i=1}^{n} k_{f,i}(\varepsilon_{pl,i}, \dot{\varepsilon}, T)\zeta_i | i = \gamma, f, p, b, m \tag{13}$$

The influence on the prediction of the part geometry due to a false prognosis of the volume fractions can be seen especially in the area of the part (see Fig. 8) that is graded in its mechanical properties. If the amount of ferrite is overpredicted, as with *MAT_244 (Livermore Software Technology Corporation, 2014), the calculated stress state yields to a plastification that results in a non-realistic deformation (Fig. 13(a)). The plastification can only be prevented taking into account the hardening effects due to the prediction of higher amounts of perlite and bainite calculated with material model *MAT_248. Thus, the total displacement can be predicted in good accordance to the optically measured data (Fig. 13(b)) of the indirect hot stamped b-pillar.

So, this example shows the necessity for the correct prediction of the composition of the volume fractions, phase transformation induced strains and plasticity and the hardening over the entire process of annealing. The results presented in this work point up the need for the thermo-mechanical metal–physical coupling, especially, for taking into account the discussed effects of supercooling austenite. This is mandatory for the prediction of the different volume fractions that are essential for calculating the mechanical

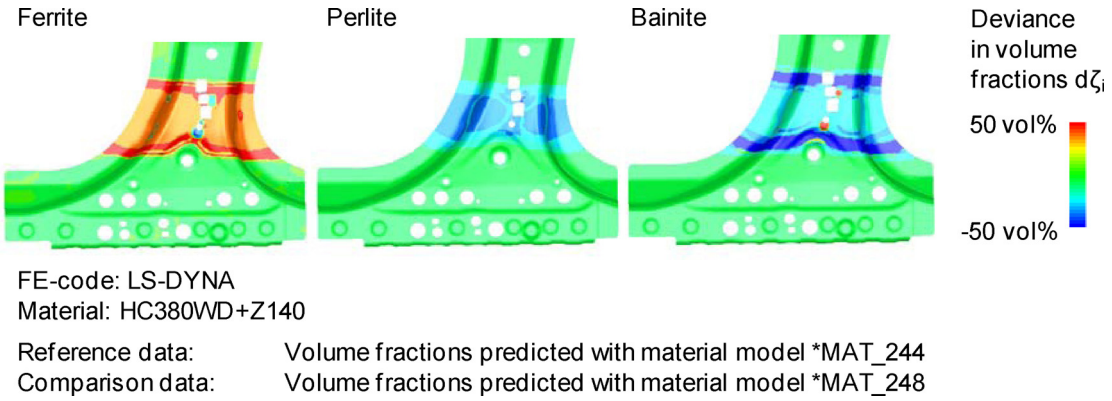

Fig. 10. Difference plots of volume fractions of ferrite, perlite and bainite due to a diffusion controlled phase transformation predicted with material model *MAT_244 and material model *MAT_248

Livermore Software Technology Corporation (2014).

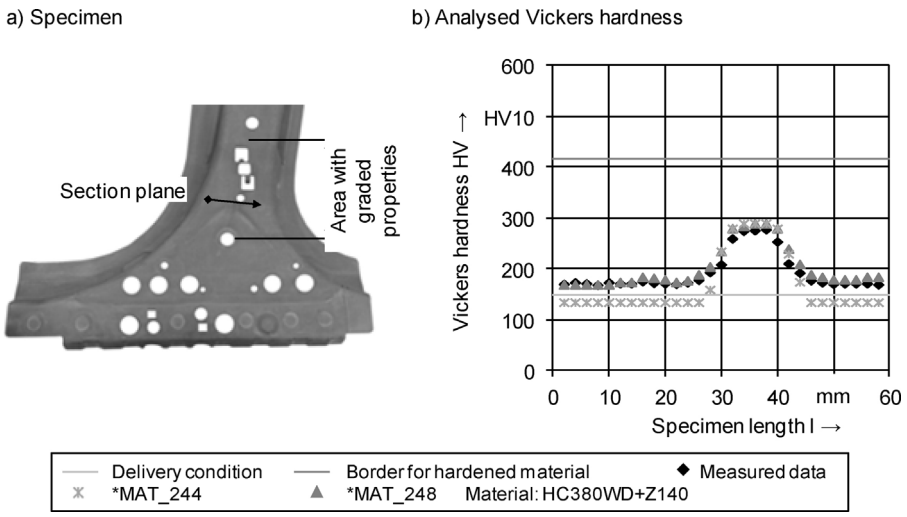

Fig. 11. (a) Specimen and location of the section planes where the Vickers hardness was analysed by measurement and FE-simulations with material model *MAT_244 and *MAT_248
Livermore Software Technology Corporation (2014).

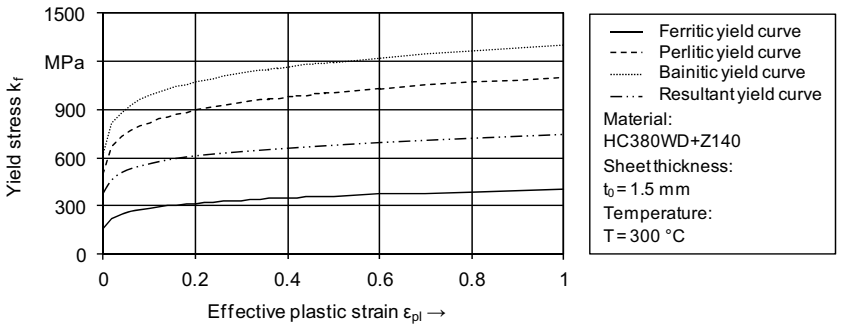

Fig. 12. Calculated yield stress k_f in dependency on the effective plastic strain for ferrite, perlite and bainite at 300 °C and the resultant yield curve $k_f(\varepsilon_{pl})$ by using a mixture rule for the phases.

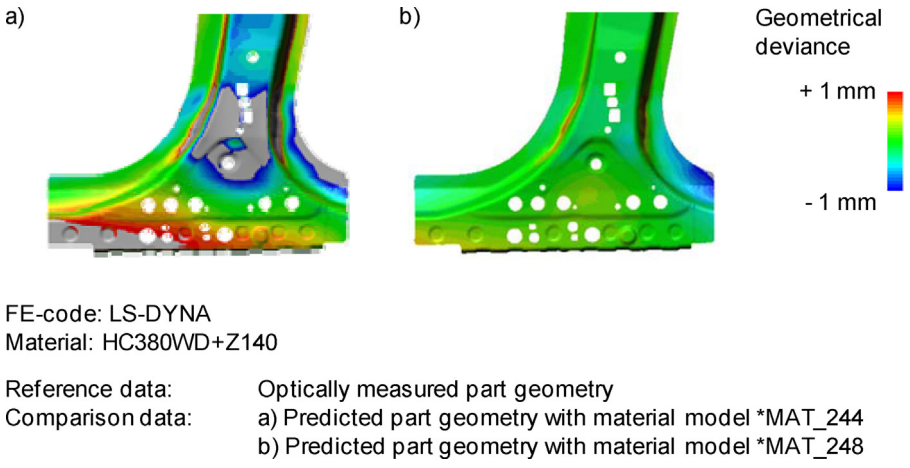

Fig. 13. Predicted part geometry with material model *MAT_244 (left) and material model *MAT_248 (right) (Livermore Software Technology Corporation, 2014) in comparison to the optical measured data.

properties and the material hardening behaviour in order to be able to predict the part geometry.

Conclusion

The present study aimed at modelling kinetics of phase transformation for the prediction of the part geometry and mechanical properties of indirect hot stamped car body parts with tailored properties. Therefore, a material model was developed considering diffusionless and diffusion controlled kinetics of phase transformation. For springback simulation immediately after the hardening process and for the simulation of thermal deformations, while supercooling to room temperature, the actual strain and stress state is mandatory information. Due to its dependency on

the actual volume fractions the phase transformation model was coupled with a thermo-mechanically coupled material model, considering phase transformation induced strains and stresses. For industrial application the material model was implemented in the FE-code LS-DYNA 971 and will be released as material model *MAT_248. Material model *MAT_248 includes:

- a new model for calculating the evolution of martensite,
- an individual choice of evolution parameters for each phase,
- an approach for calculating the volume fractions of ferrite and perlite in equilibrium,
- an approach for calculating transformation induced strains for each phase transformation
- and a density calculation of individual phases.

It has been shown that the quality of prediction of the part geometry and mechanical properties can be improved significantly by the use of the modified phase transformation models, which take the metal–physical effects occurring over the entire process of hot stamping into account.

References

Åkerström, P., (Ph.D. thesis) 2006. Modelling and Simulation of Hot Stamping. Lulea University of Technology.

Banik, J., Lenze, F., Sikora, S., Laurenz, R., 2011. Tailored properties – a pivotal question for hot forming. In: Steinhoff, K., Oldenburg, M., Prakash, B. (Eds.), Proceedings of 3rd International Conference of Hot Sheet Metal Forming of High-Performance Steel. Kassel, pp. 13–20.

BÄHR-Thermoanalyse GmbH, 2014. http://www.mpa.mw.tum.de/fileadmin/tumwmpa/www/MPA/pdf/Dilatometer_Produktblatt.pdf (15.04.14).

Bathe, K., 2002. Finite-Elemente-Methoden. Springer Verlag, Berlin/Heidelberg/New York.

Bechet Beaujard, 2003. ISO 643.2003. Steels – Micrographic Determination of the Apparent Grain Size.

Behrens, B.-A., Bouguecha, A., Götze, T., Schrödter, J., 2012. Neue entwicklungen beim formhärten. In: Merklein, M. (Ed.), 7. Erlanger Workshop Warmblechumformung. Erlangen, pp. 133–151.

Bergman, G., Oldenburg, M., 1997. Verification of thermomechanical material models by thinplate quenching simulations. J. Therm. Stress. 20, 679–695.

Bergman, G., Oldenburg, M., 2004. A finite element model for thermomechanical analysis of sheet metal forming. Int. J. Numer. Methods Eng. 59, 1167–1186.

Finkler, T., Marx, A., Graff, S., Banik, J., Sikora, S., Lenze, F.-J., 2013. Kompetenz in der Warmumformung – State of the art – Werkstoff-, Prozess- und AnlagentechnikAktueller Stand und zukünftiger Forschungsbedarf. In: Merklein, M. (Ed.), 8. Erlanger Workshop Warmblechumformung. Erlangen, pp. 1–20.

George, R., Bardelcik, A., Worswick, M.J., 2011. Hot forming of a lab-scale b-pillar with tailored properties – experiment and modelling. In: Oldenburg, M., Steinhoff, K., Prakash, B. (Eds.), 3. International Conference on Hot Sheet Metal Forming of High-Performance Steel. Wissenschaftliche Scripten, Auerbach, pp. 31–37.

Hippchen, P., Merklein, M., Lipp, A., Fleischer, M., 2012a. Aktuelle Entwicklungen in der FE-Simulation des indirekten Presshärteprozesses bei der BMW Group. In: DYNAmore GmbH (Ed.), 11. LS-DYNA Forum. Ulm, Germany, pp. 84–86.

Hippchen, P., Merklein, M., Lipp, A., Fleischer, M., Grass, H., Craighero, P., 2012b. Untersuchung und Modellierung des Gefügeumwandlungsverhaltens für das indirekte Presshärten unter Serienprozessbedingungen. In: Merklein, M. (Ed.), 7. Erlanger Workshop Warmblechumformung. Erlangen, pp. 133–151.

Hippchen, P., Merklein, M., Lipp, A., Fleischer, M., Grass, H., Craighero, P., 2013. Modelling kinetics of phase transformation for the indirect hot stamping process. In: Clarke, R.B., Leacock, A.G., Duflou, J.R., Merklein, M., Micari, F. (Eds.), Main Theme: Sheet Metal 2013 Key Engineering Materials, vol. 549, pp. 108–116, Switzerland.

Hochholdinger, B., (Ph.D. thesis) 2012. Simulation des Presshärteprozesses und Vorhersage der mechanischen Bauteileigenschaften nach dem Härten. ETH Zurich, Zurich, Switzerland.

Hultgren, A., 1938. Diskussion über "The Physics of Hardenability" von R.F. Mehl. Hardenability of Alloy Steels., pp. 55–56.

Jablonka, A., Harste, K., Schwerdtfeger, K., 1991. Thermodynamical properties of iron and iron-carbon alloys: density and thermal contraction. Steel Res. 62, 24–33.

Karbasian, H., Tekkaya, A.E., 2010. A review on hot stamping. J. Mater. Process. Technol. 210, 2103–2118.

Kirkaldy, J.S., Venugopalan, D., 1983. Prediction of microstructure and hardenability in low alloy steels. In: Marder, A.R., Goldstein, J.I. (Eds.), International Conference on Phase Transformations in Ferrous Alloys. , pp. 125–148.

Koistinen, D.P., Marburger, R.E., 1959. A general equation prescribing the extent of the austenite–martensite transformation in pure iron–carbon alloys and plain carbon steels. Acta Metall. 7, 59–60.

Lee, S.-J., Pavlina, E.J., Van Tyne, C.J., 2010. Kinetics modeling of austenite decomposition for an end-quenched 1045 steel. Mater. Sci. Eng. A 527, 3186–3194.

Li, V., Niebuhr, D., Meekisho, L., Atteridge, D., 1998. A computational model for the prediction of steel hardenability. Metall. Mater. Trans. B 29, 661–672.

Livermore Software Technology Corporation, 2006. LS-Dyna Theory Manual, Version 2006. Livermore Software Technology Corporation.

Livermore Software Technology Corporation, 2014. LS-Dyna Keyword User's Manual, Volume, II, Material Models, Version 971/Release 6. Livermore Software Technology Corporation.

Miettinen, J., 1997. Calculation of soldification-related thermophysical properties for steel. Metall. Mater. Trans. B 28B, 281–297.

Mori, K., 2012. Smart hot stamping of ultra-high strength steel parts. Trans. Nonferr. Met. Soc. China 22, 496–503.

Olle, P., (Ph.D. thesis) 2010. Numerische und Experimentelle Untersuchungen zum Presshärten. Leibniz Universität Hannover, Hannover, Germany.

Trapp, N., (Ph.D. thesis) 2010. Methoden und Strategien zur Simulation der Wärmebehandlung komplexer Bauteile aus 20MnCr5. Universität Karlsruhe, Karlsruhe. Fakultät für Maschinenbau.

Voestalpine Stahl GmbH, 2014. Material Data Sheet, http://www.voestalpine.com/division_stahl/content/download/3987/30705/file/DB_phs-ultraform_1500Z140_D_12032013.pdf (15.04.14).

Zhao, L., Dijk, N., Brück, E., Sietsma, J., Zwaag, S., 2001. Magnetic and X-ray diffraction measurements for the determination of retained austenite in TRIP steels. Mater. Sci. Eng. A313, 145–152.